# Lineshape estimation for magnetic resonance spectroscopy (MRS) signals: self-deconvolution revisited

**D M Sima[1], M I Osorio Garcia[1], J Poullet[1], A Suvichakorn[2], J-P Antoine[2], S Van Huffel[1], D van Ormondt[3]**

[1] Department of Electrical Engineering ESAT-SCD, Katholieke Universiteit Leuven, Kasteelpark Arenberg 10, 3001 Leuven-Heverlee, Belgium
[2] SC/PHYS/FYMA, Université Catholique de Louvain, Louvain-la-Neuve, Belgium
[3] Department of Applied Physics, Delft University of Technology, Delft, The Netherlands

E-mail: diana.sima@esat.kuleuven.be

**Abstract.** Magnetic Resonance Spectroscopy (MRS) is an effective diagnostic technique for monitoring biochemical changes in an organism. The lineshape of MRS signals can deviate from the theoretical Lorentzian lineshape due to inhomogeneities of the magnetic field applied to patients and to tissue heterogeneity. We call this deviation a distortion and study the self-deconvolution method for automatic estimation of the unknown lineshape distortion. The method is embedded within a time-domain metabolite quantitation algorithm for short-echo time MRS signals. Monte Carlo simulations are used to analyze whether estimation of the unknown lineshape can improve the overall quantitation result. We use a signal with 8 metabolic components inspired by typical MRS signals from healthy human brain and allocate special attention to the step of denoising and spike removal in the self-deconvolution technique. To this end we compare several modelling techniques, based on complex damped exponentials, splines and wavelets. Our results show that self-deconvolution performs well, provided that some unavoidable hyper-parameters of the denoising methods are well-chosen. Comparison of the first and last iterations show an improvement when considering iterations instead of a single step of self-deconvolution.

*Keywords*: Magnetic Resonance Spectroscopy (MRS), lineshape distortion, self-deconvolution
Submitted to: *Meas. Sci. Technol.*

## 1. Introduction

*In vivo* Magnetic Resonance Spectroscopy (MRS) is a noninvasive technique that can be used for monitoring metabolites in a tissue. It is an effective tool for diagnosis of major diseases. MRS signals are measured in the time domain as complex-valued decaying signals. For visualisation purposes they are usually Fourier transformed to the frequency domain, yielding MR spectra. A perennial point of concern is that static and dynamic inhomogeneity of the magnetic field distorts the natural lineshape of the spectral components. This lineshape is determined by the damping of the time-domain signal components. Ideally, the damping function of metabolites in a liquid solution is a decaying exponential, but under *in vivo* conditions the damping function is *a priori* unknown due to the mentioned inhomogeneity of the applied magnetic field, which in turn is mainly due to the heterogeneity of patient's tissue. This complicates signal analysis and might compromise the estimation of important parameters, if it is not appropriately taken into account.

Metabolite quantitation of an MRS signal aims at determining the concentration of each metabolite present in the region under investigation. Traditionally, quantitation methods based on a model function [1, 2] assume a Lorentzian lineshape for each spectral component, or correspondingly, complex damped exponential components in the time domain. Alternative models include Gaussian or Voigt lineshapes, the latter being a combination of Lorentzian and Gaussian functions. Only a few quantitation methods allow more freedom to the lineshape. In order to apply any model-based quantitation method that allows only analytic lineshapes such as Lorentzian, Gaussian or Voigt, it is assumed that the raw data is preprocessed to become suitable for analysis, such that the modified signals match the analytic model [3]. However there are some algorithms that allow freedom of the lineshape during the quantitation itself by using non-analytical models [4, 5].

A typical assumption of the methods that deal with the lineshape is that all spectral components in the signal are affected by the same spectral distortions. Restrictions to this assumption include differential chemical shift changes caused by temperature fluctuations, or perturbations caused by weak radiofrequency fields, which cannot be corrected [6].

A fundamental difference between lineshape correction methods concerns whether they use a *reference signal* or they do not. Methods such as *reference deconvolution* need a reference signal, which is either a separate measurement, or a spectral component extracted from the analyzed signal. First the experimental signal is deconvolved with the reference signal. Then the resulting signal may be fitted by an ideal analytic model. Reference deconvolution was proposed independently by several authors; here we mention the FIDDLE (free induction decay deconvolution for lineshape enhancement) method proposed in [7] (see also [8]) and the QUALITY (quantification improvement by converting lineshapes to the Lorentzian type) method proposed in [9]. Further developments for automating these methods have been proposed in [10, 11]. The problem

of these methods is the potential risk of dividing by zero, which introduces a spike effect.

In [12], a method inspired by [9] and [13], from which it takes its name QUECC, is meant to benefit from the advantages of both methods, **QU**ALITY [9] for a complete correction of the lineshape such that it matches a decaying exponential and Klose's eddy current correction method (**ECC**) [13] for avoiding the spike effect. The signal is separated in two parts defined by a cross-over point in the time domain which depends on the slope and the signal-to-noise ratio (SNR) of points in the time domain reference data. The first part of the signal is corrected using QUALITY deconvolution, while the second part is corrected using ECC. To avoid discontinuity in the signal, an exponential damping constant is evaluated to equalize the magnitude of the last point which was QUALITY deconvolved with the magnitude of the first ECC point.

When the goal of lineshape estimation is improving the quantitation results rather than visually correcting the spectrum, it is better to include the reference signal as part of the quantitation method. Thus, instead of deconvolving the experimental signal, the lineshape should be incorporated into the fit by multiplying the analytic lineshapes or the metabolite profiles in the time domain with the reference lineshape (see, e.g., [5]). From a numerical point of view, this alternative is much more reliable than the deconvolution-based methods.

In the present text we consider the case when *no reference signal* is known or can be reliably extracted from the signal under investigation. Two trends for dealing with this situation can be distinguished. The first one is the incorporation of non-analytic (non-parametric) models for the lineshape using polynomials, sinusoids, or splines, for example. An extreme non-analytic representation consists in seeing the whole lineshape as an unknown vector which should be convolved during the fit with the metabolite profiles in the frequency domain (see [14] for more details). Complex undamped exponentials modelled in the time domain, which are the equivalent of Dirac delta functions in the frequency domain, are used in [5]. There is an unavoidable problem with this kind of approaches. The quantitation problem becomes ill-posed due to too many degrees of freedom and should be regularized. This always involves the fine tuning of certain hyper-parameters.

In [15], Maudsley proposed another method which does not require the use of a reference signal. The method is iterative and based on an initial estimate of the parameters of the spectral components. It is called "self-deconvolution" and it can be seen as an extreme case of reference deconvolution with multiplet signals [6] when the reference signal is the whole experimental signal itself.‡

In this paper we extend the self-deconvolution approach [15] by combining it with a quantitation method based on metabolite profiles instead of individual spectral components. Due to this extension, self-deconvolution can be successfully applied to lineshape estimation of *short-echo time* MRS signals.

‡ Note that in other branches of the literature (e.g., chemometrics) the term *Fourier self-deconvolution*, originating in [16], is used in the meaning of simple *reference deconvolution* and thus differs from the self-deconvolution method described by Maudsley [15] and considered in this paper.

An important feature of this paper is that, except for visualisation purposes, the discussion is kept exclusively in the time domain, which is the measurement domain. The terminology is however slightly loose in this respect: the terms convolution and deconvolution are usually employed when referring to spectra, but here we also mean pointwise multiplication and division of time series, respectively. Moreover, note that *lineshape* is a property of spectral components, while the corresponding concept in the time domain is the *damping function*.

The added value of the lineshape estimation method under investigation is two-fold. First, the method is applicable to short-echo time MRS signals, due to the use of metabolite profiles in the quantitation algorithm. Secondly, the method is fully automatic, due to the use of hyper-parameter selection methods in the essential step of spike removal. We give details and compare several approaches based on complex damped exponentials, splines and wavelets. Results show that each technique performs well when hyper-parameters are optimized. For their simplicity, full automation and excellent performance, we recommend the smoothing splines.

In Section 2 we discuss the theory of self-deconvolution and present some details on the quantitation algorithm. Attention will be devoted in Section 2.4 to smoothing or denoising methods aimed at overcoming the spike effect.

The methods under study are validated in Section 3 by a series of Monte Carlo simulations on simulated signals with 8 metabolic components, inspired by typical MRS signals from healthy human brain. The ultimate goal of our simulations is evaluating the improvement of metabolite quantitation when the lineshape is estimated.

The paper concludes with a discussion on the specific features of our self-deconvolution approach in relation to alternative methods.

## 2. Methods

### *2.1. Lineshape estimation by self-deconvolution*

For the presentation of the basic self-deconvolution method we follow the approach in [15], with the difference that we do all computations in the time domain.

We assume that the experimental signal $y(t)$ is composed of a sum of undistorted and possibly undamped spectral components $y_{\text{undistorted}}(t)$, multiplied by a common complex-valued damping function $g(t)$, which gives the lineshape when Fourier transformed to the frequency domain. The damping function is assumed to be normalized such that $g(t_0) = 1$, where $t_0$ is the first time index of the experimental signal. Then we have

$$y(t) = y_{\text{undistorted}}(t)\, g(t). \tag{1}$$

The self-deconvolution method proceeds as follows [15]:

(i) A preliminary spectral analysis of the original signal is carried out, where the lineshape is assumed to be analytical (Lorentzian, Gaussian, or Voigt).

(ii) The fitted model is converted into an undistorted version $\hat{y}_{\text{undistorted}}$, by reconstructing a signal from the estimated spectral parameters and ignoring the damping part.

(iii) The damping function is estimated with the **ratio formula**

$$\hat{g}(t) = \frac{y(t)}{\hat{y}_{\text{undistorted}}(t)} \tag{2}$$

(iv) Numerical instability caused by noise and division by small numbers is tackled by a smoothing of $\hat{g}(t)$, giving $\hat{g}_{\text{denoised}}(t)$.

(v) Spectral analysis of the original signal is carried out again by using the function $\hat{g}_{\text{denoised}}(t)$ as the exact damping function.

(vi) steps (ii)-(v) are repeated until convergence of the spectral parameters or of the damping function estimate.

In steps (i) and (v), the model parameters can be obtained by any spectral fitting method. In the next subsection we focus on the quantitation method AQSES [17] and we emphasize particularities of this approach.

Step (iv) is one of the most stringent issues of this algorithm and it is discussed further at length.

### *2.2. The quantitation method AQSES*

Spectra of metabolites that are visible in *in vivo* spectroscopy can be measured *in vitro* or they can also be simulated using quantum mechanical knowledge [18, 19], and these signals can be grouped in a basis set of metabolite profiles. An *in vivo* time-domain signal has, in theory, the shape of a sum of complex damped exponentials. Instead of modelling these individual components, the *in vivo* short echo time MRS signal can be modelled using the profiles in the basis set, such that the prior knowledge that relates individual peaks in the *in vivo* spectrum is implicitly imposed. The quantities of interest, the metabolite *concentrations*, can be estimated from the weighting coefficients (amplitudes) of the linearly combined *in vitro* profiles. The linear combination should allow small corrections in spectral parameters like frequency shifts, damping corrections and phase shifts, since these parameters may vary from measurement to measurement [20].

Quantitation methods also take into account the presence of a partially suppressed water resonance and the presence of the macromolecular baseline. The frequency region where the water is located is known, while the macromolecular baseline overlaps with the metabolites of interest. Typically, the quantitation methods assume that the water resonance is removed in a *preprocessing step*, using a frequency selective method. For instance, the HSVD (Hankel singular value decomposition) method [21] can be used for this purpose.

*2.2.1. The model.* We consider that we are given a metabolite basis set as a set $\{v_k, \text{ for } k = 1, \ldots, K\}$ of complex-valued time series of length $m$, representing *in*

*vitro* measured or quantum mechanically simulated MRS responses. When lineshape distortions, baseline and water contributions are ignored, we assume that an *in vivo* measured MRS signal $y$ satisfies the model

$$y(t) = \overline{y}(t) + \varepsilon_t, \quad t = t_0, \ldots, t_{m-1}, \qquad \text{with} \tag{3}$$

$$\overline{y}(t) = \sum_{k=1}^{K} a_k \exp(j\phi_k)\, \exp(-d_k t - g_k t^2 + 2\pi j f_k t)\, v_k(t), \tag{4}$$

where $a_k$ are real amplitudes, $\phi_k$ are phase shifts, $d_k$ are Lorentzian damping corrections, $g_k$ are Gaussian damping corrections, $f_k$ are frequency shifts, and $j = \sqrt{-1}$. Note in this model that the metabolite profiles $v_k$ are not simply summed up in a linear combination, since *frequency shifts, phase corrections and Voigt lineshape corrections* are specified by the nonlinear factor $\exp(j\phi_k)\exp(-d_k t - g_k t^2 + 2\pi j f_k t)$. In (3), the term $\varepsilon_t$ denotes an unknown noise perturbation with zero mean.

*2.2.2. The fitting problem.* A nonlinear least squares problem is solved for the parameters $a_k, \phi_k, d_k, g_k, f_k$:

$$\min \sum_{t=t_0}^{t_{m-1}} |y(t) - \overline{y}(t)|^2, \tag{5}$$

where $\overline{y}$ is given in (4).

As explained in [17], a variable projection [22] implementation is used in AQSES, which is computationally more efficient than optimizing the nonlinear least squares problem (5) directly over all linear and nonlinear parameters without separation. Another advantage of variable projection is that it is more robust since it does not encounter numerical problems when some amplitudes $a_k$ are nearly zero. Moreover, the Levenberg-Marquardt algorithm needs good initial values for its variables; it was found convenient to set initial values of zero for all the nonlinear parameters – frequency and damping corrections –, which means that the optimisation starts with no spectral corrections to the signals in the basis set, which are assumed to be reasonably aligned in frequency and, for the purpose of lineshape correction, to have similar dampings. A FORTRAN 77 implementation with Java interface is available in AqsesGUI [17], but the results in this paper use a Matlab version of AQSES implemented in the package SPID [23].

### *2.3. Self-deconvolution combined with AQSES*

In order to combine the self-deconvolution approach with the metabolite quantitation method AQSES, the adaptations are straightforward. Instead of a spectral analysis based on individual Lorentzian, Gaussian or Voigt components (see steps (i) and (v)), a nonlinear least squares fit with the metabolite-based model (4) is performed.

For a good initialization of the common damping function, the initial nonlinear least squares fit (step (i)) uses a constraint of equal damping corrections. That is, all

parameters $d_k$ in (4) are equal to each other, and all $g_k$'s are equal to each other, in case Voigt corrections are imposed.

When applying the ratio formula in step (iii), the denominator is reconstructed from the metabolite profiles, similarly to the formula (4) but disregarding the damping correction:

$$\hat{y}_{\text{undistorted}}(t) = \sum_{k=1}^{K} a_k \exp(j\phi_k)\, \exp(2\pi j f_k t)\, v_k(t). \tag{6}$$

Subsequent spectral analyses (step (v)) during the iterations of the self-deconvolution algorithm are done with the nonlinear least squares method AQSES using a modified basis set where each metabolite profile is pointwise multiplied by the currently estimated damping function $\hat{g}_{\text{denoised}}$. It is worth mentioning that $\hat{g}_{\text{denoised}}$ is always scaled such that its first element is 1, in order to avoid a scaling indeterminacy that can possibly lead to divergence of the method. Otherwise any arbitrary scaling factor can multiply $\hat{g}_{\text{denoised}}$ and all metabolite amplitudes can be divided by the same factor.

Finally, after convergence of the self-deconvolution iterations, we allow one final quantitation, where the metabolite basis set is corrected by the converged damping function, but where we also allow small Voigt variations of the lineshape for each metabolite separately, to account for possible lineshape imperfections that are not common and could not have been taken into account by self-deconvolution.

### *2.4. The denoising step*

An essential step in the self-deconvolution method is the denoising step, step (iv). If this step is ignored, one cannot improve upon the initial estimates that are obtained with an analytic model for the lineshape.

In this study we combine two approaches. The first one is aimed at removing spurious contributions from the tail of the estimated damping obtained through the ratio formula. The second is a modelling step aimed at denoising the rest of the damping function. Three denoising methods are evaluated in this study: sum of complex damped exponential modelling, which we name "Lorentzian modelling" for the sake of briefness, spline smoothing and wavelet denoising. They are explained in detail further in this section.

*Zeroing the tail.* The ratio formula (2) shows that for large values of the time index $t$ the estimated damping is unreliable due to the division of the tail of the experimental signal, embedded in noise, by the (possibly decayed) tail of the reconstructed signal. We emphasize that there are two possibilities: if undamped metabolite components are used to reconstruct the signal, then a stationary signal is obtained in the denominator. Thus the tail of the ratio formula is dominated simply by noise from the experimental signal. If, on the contrary, the metabolite profiles are decaying signals themselves, which is the case when they are measured *in vitro*, then the tail of the ratio formula blows up, since division of white noise to almost zero values occurs. Thus, in both cases, the tail of the

ratio is not reliable and we decide to artificially set it to zero. We must however define a cross-over point after which the tail of the damping obtained from the ratio formula can be ignored. This point is automatically chosen by relying solely on the experimental signal (i.e., the numerator), as a time index where the experimental signal is completely decayed into the noise.

The obtained damping function is further denoised with one of the following three approaches.

*2.4.1. Lorentzian modelling.* The first idea is to model the lineshape by representing a non-Lorentzian lineshape as a superposition of several Lorentzian lineshapes. To this end, we use the subspace-based method HSVD [21], which enables one to model any non-exponential signal accurately, subject to the noise level [24]. We use in particular the HLSVD-PRO implementation [25] available is SPID [23]. HSVD requires computing the truncated singular value decomposition (SVD) of a Hankel matrix $H$, containing the noisy signal in its first column and row.§ If the signal is a sum of $K$ complex damped exponentials (giving $K$ Lorentzian peaks, when the signal is Fourier transformed to the frequency domain), then the data matrix $H$ has rank exactly equal to $K$. Noise in the signal or a signal not satisfying the exponentially decaying model yields a full rank matrix $H$. By truncating the SVD to lower rank, one can approximately model a non-exponential signal as a sum of many complex damped exponentials.

When a large model order is requested, HSVD models the unwanted components such as the spikes and the noise, as well. In order to denoise the noisy damping $\hat{g}$ in (2), it is thus possible to over-parameterise this model and to subsequently select from the sum of damped exponentials only the ones that correspond to our prior knowledge about the lineshape: the lineshape distortion does not spread across the whole frequency range, but it is centered at zero. Thus we consider a pass band of the form $(-\epsilon_1, \epsilon_2)$, where the values of $\epsilon_1, \epsilon_2 > 0$ can be tuned. In our numerical experiments we use the following automatic approach: First, the noisy $\hat{g}$ is fitted by HSVD with a number $K$ of Lorentzian components ($K$ equals 10 in the experiments). The fitted Lorentzian components are arranged according to increasing absolute value of the frequency. In order to automatically select a good reconstruction, several approximations are computed, starting with the lowest frequency component, and subsequently including more and more components of higher frequency into the model. Several model selection criteria can be used for choosing the number of components; here we mention Bayesian information criterion, the L-curve, Akaike's information criterion and its second order correction. For their brief description and further references, we refer to [26]. The residual sum of squares for each approximation, as well as a measure of the model's complexity, are evaluated and a trade-off is chosen. In order to overcome possible bias of a particular model selection criterion, we take the median value of the number of components recommended by the four methods just mentioned.

§ We use a square or almost square matrix $H$, although rectangular matrices are also allowed.

*2.4.2. Wavelet denoising.* Discrete wavelets [27] can also be used for signal denoising. A signal is decomposed into a low resolution approximation plus a combination of building blocks, which are translated and/or dilated versions of the same basic function called mother wavelet. Some of the obtained wavelet coefficients correspond to details in the data set such as the noise, while others correspond to the large features in the data. Wavelet thresholding means setting to zero all coefficients that are less than a particular threshold, and use an inverse wavelet transformation to reconstruct the denoised data. There are several "hyper-parameters" that might influence the wavelet denoising method: the wavelet family, which gives the shape of the mother wavelet, the number of vanishing moments, the level of wavelet decomposition, and the threshold value itself. The simplest possible wavelet family is the Haar wavelet, which is piecewise constant, hence discontinuous, and not suitable for modelling the damping function. In our experiments the Daubechies wavelet with 3 vanishing moments and 6 coefficients [27] is found to sufficiently represent polynomial behavior while maintaining the smoothness of the damping function. The level of decomposition is then automatically selected based on the correlation and smoothness of its denoised signal. Only the lowest level of the decomposition is preserved whereas coefficients in other levels are regarded as noise and set to zero. Accordingly, the whole denoising process becomes automatic.

*2.4.3. Spline smoothing.* Smoothing splines are piecewise polynomial functions that can be linearly combined to approximately fit a noisy signal. The degree of smoothness in this fit is decided either by tuning the number and shape of the spline components, or by considering a very dense spline basis and constraining the roughness of the fitted signal. We focus on the latter approach, called penalized splines [28], where a single hyper-parameter, namely the smoothing parameter, must be tuned. This parameter gives the weighting between the approximation error and the roughness measure.

The widely used B-splines are defined recursively such that, at the given knots $\tau_1, \ldots, \tau_N$, each of the functions in the B-spline basis set is $q$-times continuously differentiable, for a certain degree $q$ (usually, $q = 3$ is enough). The recursion formula reads:

$$b_i^{\{1\}}(t) = \begin{cases} 1, & \text{if } \tau_i \le t \le \tau_{i+1} \\ 0, & \text{otherwise,} \end{cases} ; \tag{7}$$

$$b_i^{\{k\}}(t) = \frac{b_i^{\{k-1\}}(t)\,(t-\tau_i)}{\tau_{i+k-1}-\tau_i} + \frac{b_{i+1}^{\{k-1\}}(t)\,(\tau_{i+k}-t)}{\tau_{i+k}-\tau_{i+1}}. \tag{8}$$

Given the noisy damping $\hat{g}(t)$, we can model it as a linear combination of $b_1, \ldots, b_n$, *i.e.*, $\hat{g}_{\text{denoised}}(t) = \sum_{k=1}^{n} c_k b_k$, by minimizing the penalized least squares function

$$\min_{\mathbf{c}\in\mathbf{R}^n} \frac{1}{m}\sum_{i=1}^{m}\left(\hat{g}(t_i) - \sum_{k=1}^{n} c_k b_k(t_i)\right)^2 + \lambda\|\Delta\mathbf{c}\|^2, \tag{9}$$

where $m$ is the number of data points (see (3)), $\Delta$ is a finite difference operator (e.g., the second order difference matrix), and $\lambda$ is a positive scalar parameter that controls

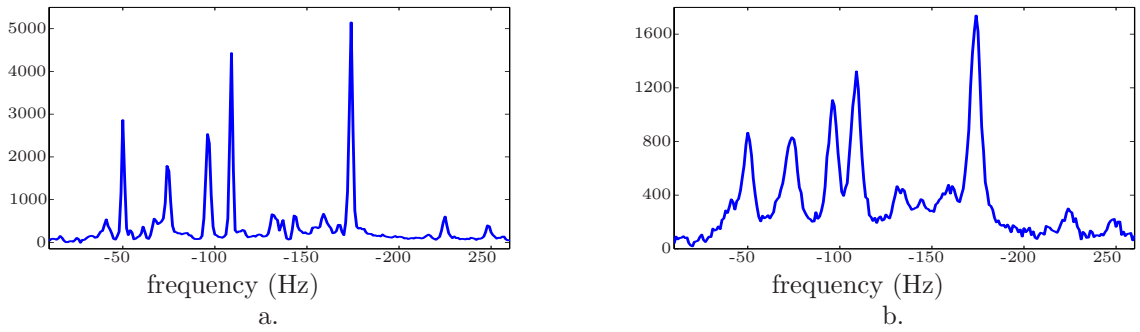


**Figure 1.** Real part of the Fourier transform of the simulated signals. a. Original undistorted signal. b. Signal distorted with the triangular lineshape and with added noise, SNR=20.

.

the degree of smoothness. $\lambda$ is called *the smoothing parameter*. The number $n$ of splines in the basis is chosen large enough such that the whole smoothing procedure is only influenced by the tuning of $\lambda$. In our experiments we take $n$ equal to a tenth of the number of data points, thus we allow one spline for every 10 data points.

There are various data-driven methods for tuning the smoothing parameter. We present here the *L-Curve*, which is a criterion developed for Tikhonov regularization of linear ill-posed problems [29] and perfectly suitable for spline smoothing. It chooses a good trade-off between minimizing the residual norm (i.e., $\sum_{i=1}^{m}\left(\hat{g}(t_i)-\sum_{k=1}^{n}c_k b_k(t_i)\right)^2$) and minimizing the value of the penalty (i.e., the (semi)norm $\|\Delta\mathbf{c}\|^2$). These two quantities are computed for a range of possible values of $\lambda$ and then plotted against each other in log-log scale. In most of the cases, a typical L-shaped plot is obtained. The $\lambda$ value corresponding to the *corner* of the obtained L-curve is chosen as optimum. These functionalities are implemented in the Matlab toolbox "Regularization Tools" [30].

### *2.5. Monte Carlo simulation procedure*

*2.5.1. Simulated signals.* Each simulated signal consisted of a combination (according to the undamped model (6)) of 8 metabolite profiles (6 metabolite profiles + 2 simulated lipid profiles) in the basis set, *i.e.*, myo-inositol (Myo), creatine (Cr), phosphocholine (PCh), glutamate (Glu), NAA, lactate (Lac), lipid at 1.3 ppm (Lip1), and lipid at 0.9 ppm (Lip2). These metabolites were chosen since they have been found to be important in the detection of many pathologies. For the simulated signals, the amplitudes were restricted to some mean values corresponding to normal tissue (see [17] for details), the phases were set variable between -45 and 45 degrees, but were the same for all profiles in one simulated signal, and the frequency shifts were restricted to zero $\pm$4.5 Hz. An illustration of such a spectrum is given in Figure 1.a.

*2.5.2. Simulated damping function.* The distortion of the damping function of *in vivo* MRS signals depends on the scanner at hand and on tissue heterogeneity at the chosen

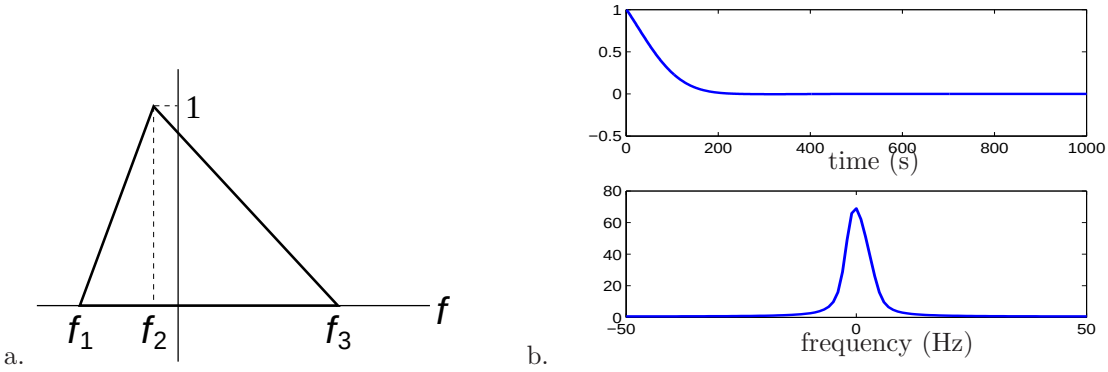


**Figure 2.** a. Simulated triangle, whose asymmetry is determined by choosing $f_2-f_1 \neq f_3-f_2$. The vertical axis indicates that the first two frequencies are negative. In the simulations we used $f_1 = -0.003$, $f_2 = -0.001$, $f_3 = 0.005$.
b. Final simulated damping function and lineshape (top: real part of the time domain signal, bottom: real part of the frequency-domain signal)

.

location in a patient. The more heterogeneous the tissue, the faster the decay of the damping function. Moreover, geometric asymmetry of the tissue distribution results in asymmetry of the spectral shape. In view of the diversity of local geometry in a patient, a spectral shape that represents all cases cannot be given. We emphasize the assumption that a common dominant contribution to the damping is present in all spectral components of the MRS signal. In this study, the spectral shape of the distortion was chosen to be asymmetric, so as to better mimic *in vivo* conditions. For easy handling of the degree of asymmetry we adopted a triangle, as shown in Figure 2; however, there are an infinite number of shapes that can be used to simulate this asymmetry. See [31] for an example of an alternative lineshape. For frequency $f$ in the interval $(f_1, f_2)$ the shape is $(f-f_1)/(f_2-f_1)$ and for $f$ in $(f_2, f_3)$, the shape is $(f_3-f)/(f_3-f_2)$; outside these regions the shape is zero. Asymmetry is achieved by setting $f_2 - f_1 \neq f_3 - f_2$. An MRS signal is measured in the time domain, hence we must calculate the Fourier transform of the shape function to arrive at the wanted damping function for the simulation. The Fourier transform of the triangular shape in Figure 2 can be analytically written as

$$f(t) = \frac{2}{f_3 - f_1} \frac{1}{2\pi j t} \left( \frac{\exp(x_1) - \exp(x_2)}{x_2 - x_1} + \frac{\exp(x_3) - \exp(x_2)}{x_3 - x_2} \right), \qquad (10)$$

for $t > 0$, where $x_i = 2\pi j f_i t$, for $i = 1, 2, 3$. The factor $2/(f_3 - f_1)$ serves as normalization. The function in equation (10) is then smoothed by pointwise multiplication with a damped exponential. The final simulated damping becomes

$$g(t) = f(t)\, \exp(-rt), \quad \text{for a certain } r > 0,$$

and is visualized in Figure 2.b.

*2.5.3. Monte Carlo procedure.* The final simulated signal (Figure 1.b.) is obtained by pointwise multiplication of the signal computed from the metabolite profiles (§2.5.1)

**Table 1.** Relative SNRs for each metabolite as a function of the SNR of the experimental signal. Values well below zero indicate that the signal is embedded in noise.

| Signal SNR \ Metabolites | Myo | Cr | PCh | Glu | NAA | Lac | Lip1 | Lip2 |
|---|---|---|---|---|---|---|---|---|
| 40 | 33 | 29 | 32 | 29 | 26 | 5 | 15 | 13 |
| 30 | 23 | 19 | 22 | 19 | 16 | -5 | 5 | 3 |
| 20 | 13 | 9 | 12 | 9 | 6 | -15 | -5 | -7 |
| 10 | 3 | -1 | 2 | -1 | -4 | -25 | -15 | -17 |

with the simulated damping function (§2.5.2), according to equation (1). White noise realisations with various SNRs (from 10 to 40 dB) are then added to the resulting signal. It is interesting to note that by considering additive noise on the experimental signal some metabolite signals are more susceptible of being embedded in noise than others. Table 1 shows the relative SNRs for each metabolite scaled by the considered amplitudes. We compute the SNR as $10\log_{10}\frac{\|y\|^2}{m\sigma^2}$, where the signal $y$ can be replaced by the metabolite signals, and $\sigma^2$ is set such that it corresponds to the desired SNR of the experimental signal.

## 3. Results

### *3.1. Illustration of the method*

First we illustrate the steps of the self-deconvolution method on an example. Consider the distorted noisy signal in Figure 1.b, having SNR=20. An initial spectral analysis with AQSES, considering only pure Lorentzian lineshape corrections and, thus, ignoring the lineshape distortion simulated in §2.5.2, gives imperfect fitting results, as shown in Figure 3.a.

Using the spectral parameters of the imperfect fit, we proceed to the damping estimation using the ratio formula (2). Figure 4 shows the steps involved in denoising the damping, as it is initially obtained with the ratio formula (2). Here we can observe the spikes caused by division to small numbers in the ratio formula and the consequent removal of those spikes according to the method described in §2.4.

The final reconstructed signal, after convergence of the iterative self-deconvolution method, is plotted in Figure 3.b. Notice that the peaks present in the residual after the initial fit with AQSES are effectively removed from the final residual, and the residual norm decreases with about 15%. Moreover, metabolite amplitudes are also improved, which will be thoroughly shown on Monte Carlo simulations in §3.3.

### *3.2. Comparison of denoising methods*

When examining the final damping functions obtained after convergence of the self-deconvolution algorithm in 100 Monte Carlo simulations we observe a higher variability

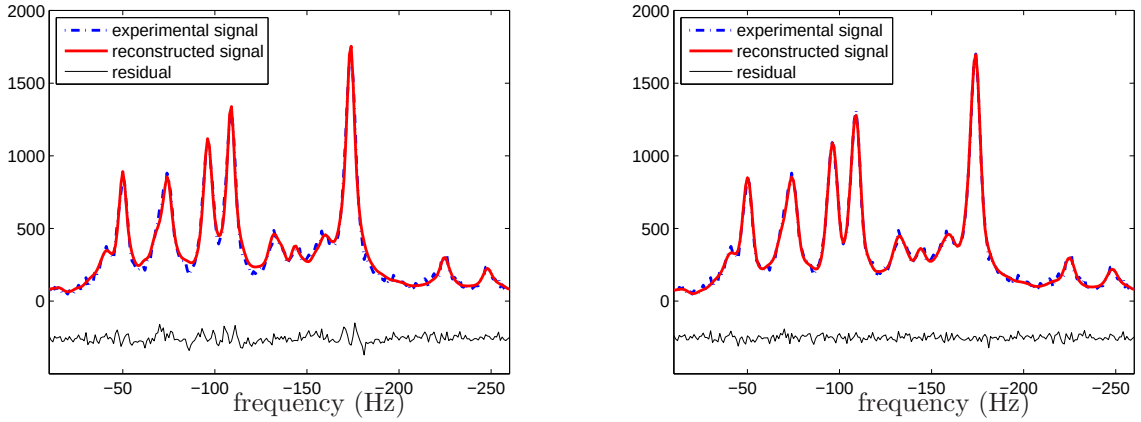


**Figure 3.** Real part of the Fourier transform of the experimental and reconstructed signals, together with the corresponding residuals. The reconstructed signals are obtained: a. after applying the quantitation method AQSES with purely Lorentzian damping corrections (norm residual/norm experimental signal = 0.1146). b. after estimation of the damping with the iterative self-deconvolution method (norm residual/norm experimental signal = 0.0985).

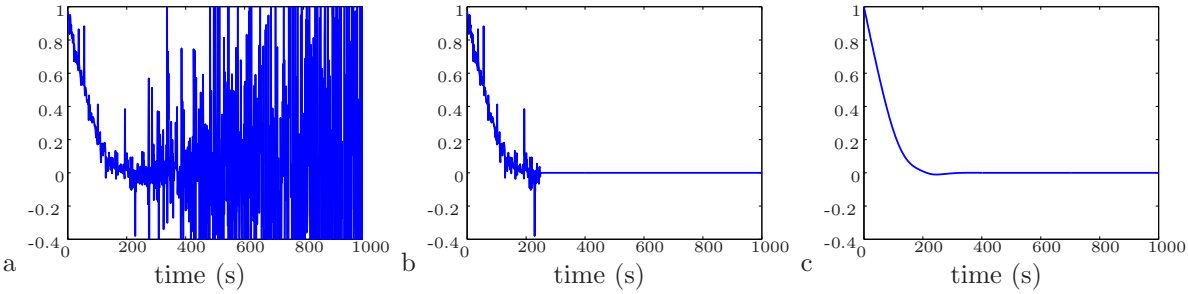


**Figure 4.** Real part of the damping signals: a. obtained from the ratio formula. b. after setting the tail to zero. c. after denoising with splines.

.

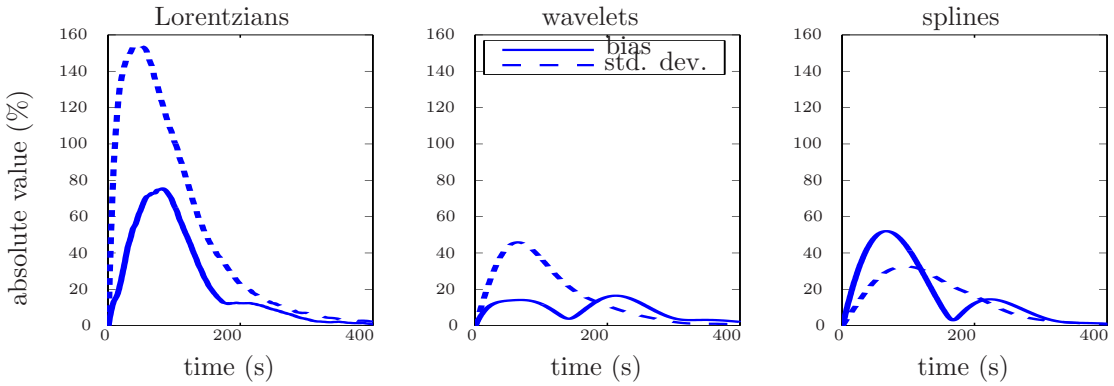


**Figure 5.** Absolute value of the pointwise standard deviation and bias with respect to the true damping function of the damping signals obtained at convergence of the self-deconvolution method, for 100 runs at SNR=10. The three plots correspond to the 3 denoising methods: Lorentzian fit, wavelet denoising, and spline smoothing, respectively. The vertical axis is scaled as a percentage of the norm of the true damping.

**Table 2.** Relative mean square errors of 100 damping function estimates, computed as $1/100 \sum_{\ell=1}^{100} \|g - \hat{g}^{\ell}_{\text{denoised}}\|^2 / \|g\|^2$.

| SNR | Lorentzians | wavelets | splines |
|---|---|---|---|
| 40 | 6.6e-3 | **3.1e-3** | 6.5e-3 |
| 30 | 5.3e-3 | **2.8e-3** | 7.8e-3 |
| 20 | 1.4e-2 | **3.7e-3** | 1.0e-2 |
| 10 | 1.4e-1 | **1.3e-2** | 2.0e-2 |

**Table 3.** Relative mean square errors of the central difference approximation of the second derivative of the damping function estimates, computed as $1/100 \sum_{\ell=1}^{100} \|D^2 g - D^2 \hat{g}^{\ell}_{\text{denoised}}\|^2 / \|D^2 g\|^2$, with $D^2 g(t_i) = g(t_{i-1}) - 2g(t_i) + g(t_{i+1})$.

| SNR | Lorentzians | wavelets | splines |
|---|---|---|---|
| 40 | 6.8e+1 | 1.0e+1 | **2.1e-1** |
| 30 | 8.0e+0 | 9.5e+0 | **2.3e-1** |
| 20 | 1.5e+2 | 6.6e+0 | **2.7e-1** |
| 10 | 2.2e+3 | 6.7e+0 | **3.7e-1** |

of the damping functions obtained from Lorentzian modelling, which indicates that the criterion of keeping low frequency damped exponentials is not perfectly suited for denoising the ratio formula. This can be seen from the pointwise bias and standard deviation plots (see Figure 5, corresponding to SNR 10). Furthermore, Table 2 reports on the relative mean square errors summed over all time points, computed from 100 noise realisations, for each considered SNR. These results indicate that wavelet denoising recovers damping functions that are the closest to the simulated one, in the mean square error sense. As we will see in the next subsection, spline smoothing, with automatically chosen level of smoothness, provides best results in terms of metabolite amplitudes. However, this is not reflected in Table 2, because the mean square error on the function value is not necessarily a good measure for the closeness between two functions. Other factors, such as the degree of smoothness, are important in this comparison. For illustration, Table 3 shows the mean square errors of the second derivative of the damping estimates with respect to the second derivative of the true damping. For such a measure, spline smoothing is indeed the best. The correlation between true and denoised dampings, and between their second derivative approximations, respectively, although not presented here, shows the same trend.

### *3.3. Monte Carlo results for quantitation*

In this section we show results of the Monte Carlo study for the final quantitation results. We basically compare the amplitudes estimated by the proposed methods at different noise levels to the simulated values of the amplitudes.

At first we consider a global measure of accuracy as follows. For each metabolite $k$ in the simulated signal number $l$, the true amplitudes $a_{k,l}$ are compared to the estimated

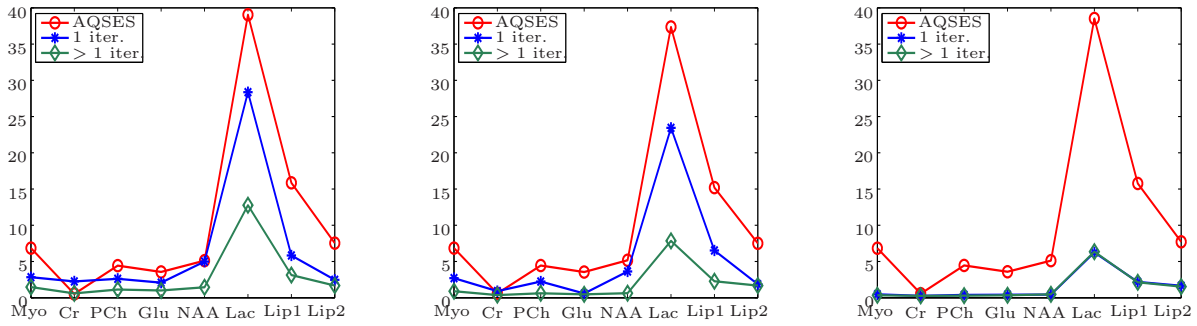


a. Lorentzians b. wavelets c. splines

**Figure 6.** Performance measure for three different methods (circles: AQSES with analytic Lorentzian lineshape, stars: one iteration of self-deconvolution, and diamonds: iterative self-deconvolution method). Results are presented for the case of SNR=30 and for the three denoising methods: a. Lorentzian-based denoising approach; b. wavelets; c. splines.

ones $\tilde{a}_{k,l}$ by means of a *performance measure* (PM) defined as:

$$\mathrm{PM}_{\mathrm{metabolite}_k} = 100\sqrt{\frac{\sum_{l=1}^{L}(a_{k,l}-\tilde{a}_{k,l})^2}{\sum_{l=1}^{L} a_{k,l}^2}}, \tag{11}$$

where $L$ is the number of simulated signals ($L = 100$). A low PM reflects a high performance, and is a percentage measure of the relative difference between estimated and true amplitudes.

Figure 6 shows results of PM comparing the estimated amplitudes after applying the quantitation method AQSES ignoring the lineshape distortion (circles), after estimation of the damping but not iteratively (stars), and after the iterative method (diamonds). The signals in this comparison have SNR=30. Large errors occur for the initial nonlinear least squares fit, where a pure decaying exponential model is assumed for the damping (the initial AQSES fit), but results always improve when applying the self-deconvolution approach. In general, we observe improvement when considering iterations, but the trend is not always obvious: when denoising with splines, the estimation is rather good from the first step; there is an improvement achieved by iterations, but this is marginal.

In order to gain better insight into the estimation accuracy, we provide, for SNRs 30 and 10, tables of relative bias and standard deviation values (*i.e.*, bias and standard deviation divided by the true amplitude for each metabolite) obtained from self-deconvolution combined with each denoising scheme. We select for illustration four metabolites with representative relative SNRs (see Table 1).

In order to illustrate the inherent limitation of the quantitation method we also present in these tables the case when amplitudes are estimated with an ideal model where each metabolite in the basis set is pointwise multiplied with the simulated damping function, as well as the Cramér-Rao lower bounds (CRB) computed from the exact parameter values and the ideal model with known damping.

**Table 4.** Relative bias and standard deviation values for the amplitudes of a selection of metabolites at SNR=30.

| Method \ Metabolites | Myo | NAA | Lac | Lip1 |
|---|---|---|---|---|
| initial | 0.0684 ± 0.0024 | 0.0355 ± 0.0023 | -0.3662 ± 0.0734 | 0.1506 ± 0.0208 |
| Lorentzians | -0.0096 ± 0.0112 | -0.0055 ± 0.0085 | 0.0438 ± 0.1199 | -0.0103 ± 0.0296 |
| wavelets | 0.0090 ± 0.0024 | 0.0042 ± 0.0027 | -0.0359 ± 0.0717 | 0.0117 ± 0.0201 |
| splines | -0.0002 ± 0.0036 | 0.0015 ± 0.0030 | 0.0012 ± 0.0579 | -0.0010 ± 0.0183 |
| known | 0.0005 ± 0.0019 | 0.0002 ± 0.0021 | 0.0083 ± 0.0669 | -0.0017 ± 0.0188 |
| true ± $\sqrt{\text{CRB}}$ | 0.0000 ± 0.0015 | 0.0000 ± 0.0021 | 0.0000 ± 0.0469 | 0.0000 ± 0.0148 |

**Table 5.** Relative bias and standard deviation values for the amplitudes of a selection of metabolites at SNR=10.

| Method \ Metabolites | Myo | NAA | Lac | Lip1 |
|---|---|---|---|---|
| initial | 0.0660 ± 0.0192 | 0.0374 ± 0.0238 | -0.0545 ± 0.5996 | 0.0842 ± 0.1795 |
| Lorentzians | 0.0239 ± 0.0910 | 0.0046 ± 0.0564 | -0.0174 ± 0.8458 | 0.0347 ± 0.2420 |
| wavelets | 0.0083 ± 0.0196 | 0.0080 ± 0.0231 | 0.1830 ± 0.5776 | -0.0240 ± 0.1684 |
| splines | 0.0044 ± 0.0196 | 0.0058 ± 0.0247 | 0.0791 ± 0.5172 | -0.0062 ± 0.1754 |
| known | 0.0031 ± 0.0151 | 0.0042 ± 0.0219 | 0.1809 ± 0.5922 | -0.0301 ± 0.1702 |
| true ± $\sqrt{\text{CRB}}$ | 0.0000 ± 0.0148 | 0.0000 ± 0.0207 | 0.0000 ± 0.4689 | 0.0000 ± 0.1484 |

For all methods, we observe, as expected, a lower standard deviation for higher SNR and the same order of magnitude between standard deviations of the self-deconvolution results, the standard deviations in the known-damping situation and the Cramér-Rao lower bounds. The accuracy is highest for the spline denoising variant, as shown by (often significantly) lower bias values.

### *3.4. Influence of hyper-parameters*

As a final experiment, we test whether the choice of hyper-parameters strongly influences the final quantitation results. These results focus on the hyper-parameter of the spline smoothing procedure, since we consider that the automated L-curve method works quite well. We run 100 noisy simulations for the following three cases: (i) the smoothing parameter $\lambda = \lambda_{\text{optimal}}$ is *optimally* chosen with the L-curve; (ii) $\lambda = 10\lambda_{\text{optimal}}$; and (iii) $\lambda = \lambda_{\text{optimal}}/10$. Two noise levels are compared in Table 6, and results show that $\lambda_{\text{optimal}}$ yields better accuracy for the amplitudes in an overwhelming majority, but the values are not bad for misspecified $\lambda$ neither.

## 4. Discussion and conclusion

Difficulties associated to the self-deconvolution approach are typically encountered in reference deconvolution, in the case of a singlet reference signal and more specifically in the case of multiplet reference signals.

Methods that deal with a singlet reference signal were faced with the problem of

**Table 6.** Performance measure (PM values) for optimal and non-optimal choice of the smoothing parameter in the case of splines. Results for SNR=10 and 30 are shown. Smaller values indicate better accuracy. Bold face marks smallest among the three values per metabolite and per SNR.

| Metab. \ $\lambda$ | SNR=30 | | | SNR=10 | | |
|---|---|---|---|---|---|---|
| | optimal | optimal×10 | optimal/10 | optimal | optimal×10 | optimal/10 |
| Myo | **0.35** | 1.89 | 0.68 | **2.03** | 5.08 | 4.92 |
| Cr | **0.27** | 0.30 | 0.53 | 2.58 | **2.41** | 2.89 |
| PCh | **0.30** | 1.25 | 0.64 | **1.78** | 3.58 | 3.96 |
| NAA | **0.34** | 1.04 | 0.69 | **2.36** | 3.87 | 4.21 |
| Glu | **0.47** | 0.90 | 1.32 | **3.85** | 5.13 | 8.13 |
| Lac | **6.36** | 10.92 | 8.98 | 58.04 | **57.21** | 63.54 |
| Lip1 | **2.13** | 4.22 | 2.57 | **16.82** | 19.75 | 19.48 |
| Lip2 | **1.53** | 2.62 | 1.73 | 15.74 | 15.93 | **15.40** |

division by almost zero values in the tail of the decaying reference signal. The method QUECC [12] addresses the fact that pointwise division can safely be performed only before a certain cross-over point. We found that such a choice of a cross-over point helps in our approach of self-deconvolution. To account for spikes in the tail of the ratio formula, which appear if we use a measured metabolite basis set consisting of damped signals, we propose to simply set the tail of the estimated damping to zero beyond a cross-over point. The cross-over point in QUECC [12] is chosen by taking into account the slope of the decaying reference signal, assumed to be a single spectral component. However, this approach does not suit the self-deconvolution method, since the signal in the denominator is not a singlet. Moreover, subsequent modelling of the damping makes any other preprocessing, such as apodization by an exponential decay, superfluous.

Deconvolution with multiplet reference signals faces also the problem of division by (close-to-)zero values before the cross-over point. This gives in practice the spike effect of the signal obtained through the ratio formula. In some special cases, such as a doublet reference signal [6], the spikes visible in discrete-time signals must be understood as discontinuities (i.e., vertical asymptotes) if the signal were to be seen in continuous time. In general there are no zeros in the denominator of the ratio formula, but relatively small values can appear. This is the case when the frequency shifts are incorrectly estimated such that the numerator and denominator cannot "cancel each other." Rapid oscillations in both signals imply that a relatively large number in the numerator might be divided by a relatively small number in the denominator, creating the spike effect.

Spikes can be removed by simple or more involved interpolation methods [15, 6]. Maudsley [15] uses an initial heuristic method for spike removal: First, to avoid dividing by zero, absolute zero points are replaced by the previous point. Further, to decrease the spike effect, the spikes are replaced by the average of the previous and next valid points. In our work, we did not find much benefit in decreasing the spike effect prior to the denoising step, thus we left the spike removal task in the hands of the denoising

method. The estimated damping is denoised by modelling in Maudsley's approach [15], as well. He proposes three variants: smoothing with Gaussian kernels; polynomial fit; and Lorentzian fit with a limited number of exponentials where a grid of frequency and decay parameters are given. We find resemblance to some of our approaches, where instead of Gaussian kernels we use Lorentzian components, and instead of polynomials we use splines, which are more versatile, since they are piece-wise polynomials whose smoothness can be easily controlled.

Comparing the denoising methods in this paper, we notice that all three methods are able to provide good results that significantly improve the estimation compared to a method that ignores the lineshape distortion. However, it is essential to have a reliable way of selecting each method's hyper-parameters in order to be able to automate the whole algorithm. For all three approaches, we restricted the number of automatically chosen hyper-parameters to a minimum of *one* single parameter. For Lorentzian modelling—the number of low frequency components; for spline smoothing—the smoothing parameter; and for wavelet denoising—the level of wavelet decomposition. We mention that these methods have other tunable parameters, but they have less influence on the results. Examples of such parameters are: the size of the Hankel matrix and the total number of components in the HSVD method, the size of the wavelet and, to some extent, the wavelet family, or the degree of the piece-wise polynomials and the number and position of the knots used in the spline approach.

Self-deconvolution combined with a quantitation method based on metabolite profiles such as AQSES [17] exhibits some advantages. Metabolite profiles incorporate prior knowledge that usually leads to excellent initial estimates for the spectral parameters of the fitted model; no user interaction such as peak picking is required. The results presented in this paper are obtained with a fully automated procedure, as opposed to the results shown for the self-deconvolution method in [15], where a peak-picking procedure was used.

Baseline contributions of macromolecules are known to be largely present in short-echo-time spectra of human brain. However, the presented self-deconvolution method does not take into account this contribution. Nevertheless, it is possible to combine lineshape estimation by self-deconvolution with baseline estimation, using either non-parametric modelling for the baseline as in AQSES [17] or truncation and subtraction as in QUEST [32]. Details are still to be worked out and will be presented elsewhere.

Finally we have to acknowledge that this study was initially motivated by an approach proposed in [33, 34], for which we suggested an improvement by considering iterations in [35]. It turned out that the same idea lies at the basis of the self-deconvolution approach introduced by Maudsley [15]. It is worth mentioning that the authors of [34] improved their initial method by constructing a purely optimisation-based approach, which avoids the need for a denoising step; this work is submitted to the same special issue as this manuscript. The two papers complement each other by taking on two different paths: the model-based and model-free approaches for accommodating the lineshape.

## Acknowledgments

Dr. Diana M. Sima is a postdoctoral fellow of the Fund for Scientific Research-Flanders. Maria I. Osorio Garcia and Dr. Aimamorn Suvichakorn are Marie Curie research fellows in the Research Training Network 'FAST' (`www.fast-mrs.eu`). Research supported by

- Research Council KUL: GOA-AMBioRICS, CoE EF/05/006 Optimization in Engineering (OPTEC), IDO 05/010 EEG-fMRI, IOF-KP06/11, several PhD/postdoc and fellow grants;
- Flemish Government:
  - FWO: PhD/postdoc grants, projects, G.0407.02 (support vector machines), G.0360.05 (EEG, Epileptic), G.0519.06 (Noninvasive brain oxygenation), FWO-G.0321.06 (Tensors/Spectral Analysis), G.0302.07 (SVM), G.0341.07 (Data fusion), research communities (ICCoS, ANMMM);
  - IWT: PhD Grants;
- Belgian Federal Science Policy Office IUAP P6/04 (DYSCO, 'Dynamical systems, control and optimization', 2007-2011);
- EU: BIOPATTERN (FP6-2002-IST 508803), ETUMOUR (FP6-2002-LIFESCIHEALTH 503094), Healthagents (IST-2004-27214), FAST (FP6-MC-RTN-035801)
- ESA: Cardiovascular Control (Prodex-8 C90242)

## References

[1] A. van den Boogaart, F. A. Howe, L. M. Rodrigues, M. Stubbs, and J. R. Griffiths. In vivo $^{31}$P MRS: absolute concentrations, signal-to-noise and prior knowledge. *NMR Biomed.*, 8(2):87–93, Apr 1995.

[2] L. Vanhamme, A. van den Boogaart, and S. Van Huffel. Improved method for accurate and efficient quantification of MRS data with use of prior knowledge. *J. Magn. Reson.*, 129:35–43, 1997.

[3] J. Poullet, D. M. Sima, and S. Van Huffel. MRS signal quantitation: a review of time- and frequency-domain methods. *J. Magn. Reson.*, 195:134–144, 2008.

[4] S. W. Provencher. Automatic quantitation of localized in vivo $^{1}$H spectra with LCModel. *NMR Biomed.*, 14(4):260–4, 2001.

[5] J. Slotboom, C. Boesch, and R. Kreis. Versatile frequency domain fitting using time domain models and prior knowledge. *Magn. Reson. Med.*, 39(6):899–911, 1998.

[6] H. Barjat, G. A. Morris, A. L. G. Wanson, S. E. Smart, and S. T. C. R. Williams. Reference deconvolution using multiplet reference signals. *J. Magn. Reson.*, 116:206–214, 1995.

[7] G. A. Morris. Compensation of instrumental imperfections by deconvolution using an internal reference signal. *J. Magn. Reson.*, 80:547–552, 1988.

[8] G. A. Morris, H. Barjat, and T. J. Horne. Reference deconvolution methods. *Prog. NMR Spectrosc.*, 31:197–257, 1997.

[9] A. A. de Graaf. QUALITY: quantification improvement by converting lineshapes to the Lorentzian type. *Magn. Reson. Med.*, 13:343–57, 1990.

[10] A. A. Maudsley, Z. Wu, D. J. Meyerhoff, and M. W. Weiner. Automated processing for proton spectroscopic imaging using water reference deconvolution. *Magn. Reson. Med.*, 31(6):589–595, Jun 1994.

[11] P. Webb, D. Spielman, and A. Macovski. Inhomogeneity correction for in vivo spectroscopy by high-resolution water referencing. *Magn. Reson. Med.*, 23(1):1–11, Jan 1992.

[12] R. Bartha, D. J. Drost, R. S. Menon, and P. C. Williamson. Spectroscopic lineshape correction by QUECC: combined QUALITY deconvolution and eddy current correction. *Magn. Reson. Med.*, 44(4):641–5, 2000.

[13] U. Klose. In vivo proton spectroscopy in presence of eddy currents. *Magn. Reson. Med.*, 14:26–30, 1990.

[14] S. W. Provencher. Estimation of metabolite concentrations from localized in vivo proton NMR spectra. *Magn. Reson. Med.*, 30(6):672–79, 1993.

[15] A. A. Maudsley. Spectral lineshape determination by self-deconvolution. *J. Magn. Reson. B*, 106(1):47–57, Jan 1995.

[16] J. K. Kauppinen, D. J. Moffatt, H. H. Mantsch, and D. G. Cameron. Fourier self-deconvolution: A method for resolving intrinsically overlapped bands. *Applied Spectroscopy*, 35(3):271–276, 1981.

[17] J. Poullet, D. M. Sima, A. W. Simonetti, B. De Neuter, L. Vanhamme, P. Lemmerling, and S. Van Huffel. An automated quantitation of short echo time MRS spectra in an open source software environment: AQSES. *NMR Biomed.*, 20(5):493–504, 2007.

[18] D. Graveron Demilly, A. Diop, A. Briguet, and B. Fenet. Product-operator algebra for strongly coupled spin systems. *J. Magn. Reson. A*, 101(3):233–39, 1993.

[19] S. A. Smith, T. O. Levante, B. H. Meier, and R. R. Ernst. Computer simulations in magnetic resonance. An object-oriented programming approach. *J. Magn. Reson. A*, 106(1):75–105, 1994.

[20] H. Ratiney, M. Sdika, Y. Coenradie, S. Cavassila, D. van Ormondt, and D. Graveron-Demilly. Time-domain semi-parametric estimation based on a metabolite basis set. *NMR Biomed.*, 18(1):1–13, 2005.

[21] W. W. F. Pijnappel, A. van den Boogaart, R. de Beer, and D. van Ormondt. SVD-based quantification of magnetic resonance signals. *J. Magn. Reson.*, 97(1):122–34, 1992.

[22] G. H. Golub and V. Pereyra. The differentiation of pseudo-inverses and nonlinear least squares problems whose variables separate. *SIAM J. Numer. Anal.*, 10:413–32, 1973.

[23] J. Poullet. *Quantification and Classification of Magnetic Resonance Spectroscopic Data for Brain Tumor Diagnosis*. PhD thesis, Faculty of Engineering, K.U.Leuven, Leuven, Belgium, 2008.

[24] R. de Beer and D. van Ormondt. *in: NMR Basic Principles and Progress*, volume 26, chapter 'Analyis of NMR data using Time-Domain Fitting Procedures', pages 201–248. Springer, 1992.

[25] T. Laudadio, N. Mastronardi, L. Vanhamme, P. Van Hecke, and S. Van Huffel. Improved Lanczos algorithms for blackbox MRS data quantitation. *J. Magn. Reson.*, 157(2):292–7, 2002.

[26] D. M. Sima. *Regularization techniques in model fitting and parameter estimation*. PhD thesis, K.U.Leuven, 2006.

[27] I. Daubechies. *Ten Lectures on Wavelets*. SIAM, 1992.

[28] P. H. C. Eilers and B. D. Marx. Flexible smoothing with B-splines and penalties. *Stat. Sci.*, 11:89–121, 1997.

[29] P. C. Hansen. Analysis of discrete ill-posed problems by means of the L-curve. *SIAM Review*, 32:561–580, 1992.

[30] P. C. Hansen. Regularization Tools, a Matlab package for analysis of discrete regularization problems. *Numerical Algorithms*, 6:1–35, 1994.

[31] A. L. Stancik and E. B. Brauns. A simple asymmetric lineshape for fitting infrared absorption spectra. *Vibrational Spectroscopy*, 47:66–69, 2008.

[32] H. Ratiney, Y. Coenradie, S. Cavassila, D. van Ormondt, and D. Graveron-Demilly. Time-domain quantitation of $^1$H short echo-time signals: background accommodation. *MAGMA*, 16(6):284–96, 2004.

[33] H. Rabeson, E. Capobianco, R. de Beer, D. van Ormondt, and D. Graveron-Demilly. Correction for $B_0$-inhomogeneity and Eddy Current effects without using a reference line. In *GRAMM*, 2008.

[34] E. Popa, D. Graveron-Demilly, E. Capobianco, R. de Beer, and D. van Ormondt. Lineshape estimation in in vivo MRS without using a reference signal. In *Proc. IEEE-IST*, pages 315–320, Chania, Greece, 2008.

[35] M. I. Osorio Garcia, D. M. Sima, J. Poullet, D. van Ormondt, and S. Van Huffel. Improvement of lineshape estimation for MRS signals. In *Proc. IEEE-IST*, pages 326–329, Chania, Greece, 2008.